

Electronic and dynamical properties of CeRh₂As₂: Role of Rh₂As₂ layers and expected orbital order


Andrzej Ptok^{1,*}, Konrad J. Kapcia², Paweł T. Jochym¹, Jan Łażewski¹,
Andrzej M. Oleś^{3,4} and Przemysław Piekarz^{1,†}

¹*Institute of Nuclear Physics, Polish Academy of Sciences, W. E. Radzikowskiego 152, PL-31342 Kraków, Poland*

²*Faculty of Physics, Adam Mickiewicz University in Poznań, Uniwersytetu Poznańskiego 2, PL-61614 Poznań, Poland*

³*Institute of Theoretical Physics, Jagiellonian University, Profesora Stanisława Łojasiewicza 11, PL-30348 Kraków, Poland*

⁴*Max Planck Institute for Solid State Research, Heisenbergstrasse 1, D-70569 Stuttgart, Germany*

 (Received 4 February 2021; revised 22 April 2021; accepted 8 July 2021; published 21 July 2021)

The recently discovered heavy fermion CeRh₂As₂ compound crystallizes in nonsymmorphic $P4/nmm$ symmetry, which enables the occurrence of topological protection. Experimental results show that this material exhibits unusual behavior, which is manifested by the appearance of two superconducting phases. In this Letter, we uncover and discuss the role of Rh₂As₂ layers and their impact on the electronic and dynamical properties of the system. The location of Ce atoms between two nonequivalent layers allows for the realization of orbital order. We point out that the electronic band structure around the Fermi level is associated mostly with Ce $4f$ and Rh $4d$ orbitals and suggest the occurrence of the Lifshitz transition induced by an external magnetic field. We discuss also the role played by the f - d orbital hybridization in the electronic band structure.

DOI: [10.1103/PhysRevB.104.L041109](https://doi.org/10.1103/PhysRevB.104.L041109)

Introduction. The recently discovered CeRh₂As₂ superconductor [1] is one of the rare examples of a heavy fermion system crystallizing in the $P4/nmm$ space group. In contrast to isostructural SrPt₂As₂ [2] or RPt₂Si₂ (where $R = Y, La, Nd, \text{ and } Lu$) [3], it does not exhibit a coexistence of superconductivity and charge density waves.

In the case of CeRh₂As₂, two anomalies in the specific heat are observed below 1 K [1]. The first anomaly (at lower temperature) is associated with the phase transition from the normal state to the superconducting (SC) phase (connected with a diamagnetic drop of the ac susceptibility and the specific heat jump of the same order of magnitude as the Bardeen-Cooper-Schrieffer value). The second anomaly (at higher temperature) is not associated with superconductivity, but likely signals some other kind of order (its T_c increases with the in-plane magnetic field). In the presence of a magnetic field perpendicular to the Rh₂As₂ layers, the system exhibits a phase transition inside the SC state. It is suggested that at the transition the parity of superconductivity changes from an even to odd one. This leads to the H - T phase diagram in a characteristic form [1], which can be treated as a generic one for a realization of spin-singlet and spin-triplet SC phases [4]. Here, we would like to emphasize that this behavior is also observed in other systems, where a coexistence of trivial and topological SC phases can occur [5–7] due to finite spin-orbit coupling (SOC), whereas the ranges in which both kinds of superconductivity exist strongly depend on the model parameters, e.g., on the ratio of electron hopping and SOC [8].

The symmetry of the system described by the $P4/nmm$ space group is nonsymmorphic with multiple symmetries protecting the Dirac points [9]. A similar situation has been

recently reported for Dirac semimetals, crystallizing in the same symmetry [10–16]. However, contrary to these materials, where a dominant role is played by the square nets [17], in the CeRh₂As₂ compound, there exist two different types of Rh₂As₂ layers (Fig. 1). What is more important, these layers can be treated as planes of the glide symmetry. The purpose of this Letter is to highlight the important role played by the Rh₂As₂ layers in the possible realization of orbital order as the result of two distinguishable Ce atom positions with respect to the neighboring Rh₂As₂ layers. We point out that the existence of this order leads to an essential modification of the phonon dispersion and could be tested by experimental measurements. We discuss also the possibility of a Lifshitz transition induced by the magnetic field as a source of the topological superconducting phase reported experimentally in Ref. [1].

The density functional theory (DFT) calculations were performed using the VASP code [18–20]. Phonon calculations were conducted by ALAMODE [21] for the thermal distribution

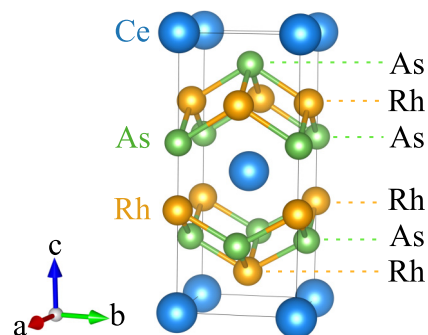


FIG. 1. The unit cell of the CeRh₂As₂ crystal structure. The system is composed of two Rh₂As₂ layers, which separately play a role of the mirrors of the glide symmetry.

* aptok@mmj.pl

† piekarz@wolf.ifj.edu.pl

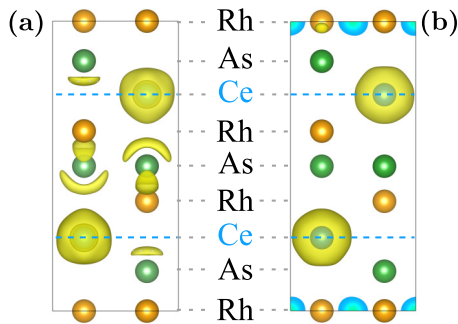


FIG. 2. (a) The electron localization function and (b) the partial charge density (for occupied states 1 eV below the Fermi level) in CeRh_2As_2 . Results were obtained in the presence of SOC and with Ce $4f$ electrons treated as valence electrons.

of multidisplacement of atoms at $T = 50$ K, generated within the high efficiency configuration space sampling (HECSS) procedure [22]. More details of the numerical calculation can be found in Refs. [23–26] and in the Supplemental Material (SM) [27].

Crystal structure. CeRh_2As_2 crystallizes in the CaBe_2Ge_2 [28] tetragonal structure (with symmetry $P4/nmm$, space group No. 129). The stacking sequence along the c axis is $\text{Ce-Rh}_2\text{As}_2\text{-Ce-Rh}_2\text{As}_2\text{-Ce}$, in which Rh_2As_2 layers are arranged in two nonequivalent forms: a square array of Rh atoms sandwiched between two checkerboard layers of As atoms (one below and one above the Rh layer, alternately) and vice versa (a square As layer decorated by Rh atoms, alternately, from top and bottom). This corresponds to the upper and lower Rh_2As_2 layers in Fig. 1.

The unit cell of the studied system consists of two formula units. From the *ab initio* calculations [with the Perdew-Burke-Ernzerhof pseudopotentials for solids (PBEsol), see the SM [27]], we find the lattice constants as $a = 4.2216$ Å and $c = 9.8565$ Å, which are in good agreement with the experimental results [1]. In the case of Ce $4f$ electrons treated as valence electrons, the ground state (GS) of the system is found to be nonmagnetic (cf. the SM [27]).

Glide symmetry. The nonsymmorphic space group of CeRh_2As_2 , unusual for heavy fermion systems [29,30], supports the realization of an unconventional SC gap in the electronic structure [31] protected by space group symmetry [32]. This space group exhibits the glide symmetry, which is here realized by the Rh and As square nets inside the Rh_2As_2 layers. Therefore, the orbitals of Ce atoms should also exhibit the glide symmetry with respect to these planes. Simultaneously, the Ce electron orbitals lose the mirror symmetry (along the c direction) due to different environments from the “top” and “bottom” sides (cf. Fig. 1). Indeed, this behavior is clearly manifested directly via the electron localization function [33–35] [Fig. 2(a)] or partial charge density [Fig. 2(b)]. As one can see in Fig. 2(a), the localization of electrons around the Ce atom (at the center of the system) does not exhibit symmetry with respect to the ab plane (marked by the dashed blue line). A similar property is observed in the case of partial charge density coming from the occupied states around the Fermi level (we take states 1 eV below the Fermi level). In consequence, both Ce atoms of the unit cell are distinguish-

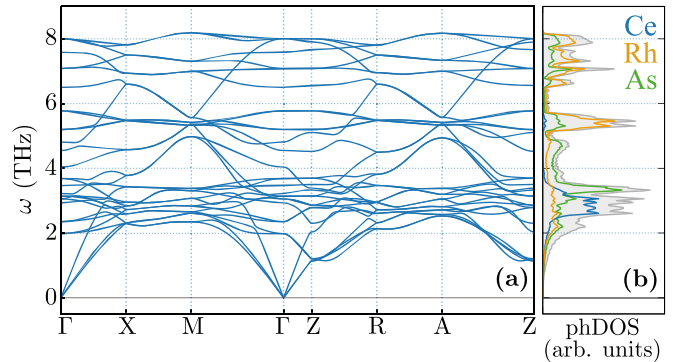


FIG. 3. Results of phonon calculations in CeRh_2As_2 : (a) Phonon dispersion curves along high-symmetry directions; (b) total and partial phonon DOS, shown by gray and color (as labeled) solid lines, respectively. Results were obtained in the presence of SOC and with Ce $4f$ electrons treated as valence electrons.

able due to the relative position with respect to the Rh_2As_2 layers and effectively realized pseudo-orbitals. This scenario is remarkably similar to URu_2Si_2 [36], where the orbitals located at the U atoms exhibit out-of-plane anisotropy and the ground state is discussed as a superposition of different irreducible representations [37] resulting in the crystal-field states [38].

In our case, orbital order can occur due to broken reflection symmetry at the Ce atoms. The onset of order in CeRh_2As_2 associated with the symmetry breaking at the Ce sites could lower the symmetry from $P4/nmm$ (space group No. 129) to $P4mm$ (space group No. 99). A similar effect of symmetry lowering can be achieved by introducing antiferromagnetic order on the sublattice of Ce atoms. This can be crucial in the context of the realization of the nontrivial topological phase, due to fact that the information about the nontrivial phase realization can be attained from the number of the bands crossing the Fermi level [39]. A changed degeneracy of the bands by symmetry modifications can lead to a different topological phase realized in the system. However, because the band structure is relatively dense and a few bands have the maxima located around the Fermi level, the results obtained in this way can be ambiguous.

Lattice dynamics. The phonon dispersion curves and densities of states (DOS) are shown in Fig. 3. As one can see, CeRh_2As_2 is stable dynamically, i.e., the soft modes (imaginary frequencies) are not observed. The irreducible representations at the the Γ point are $E_u + A_{2u}$ for acoustic modes, and $4E_u + 4A_{2u} + 5E_g + 3A_{1g} + 2B_{1g}$ for optic modes.

Partial DOS clearly show that the modes associated with the Ce atoms are located mostly at lower frequencies in a range of 2–3 THz. This is a typical behavior observed in clathrates [40], when some heavy atoms are located inside a “cage.” In our case, Ce is located inside a cage-like dodecahedron constructed by two Rh_2As_2 layers (cf. Fig. 1). Indeed, similar behavior is observed, e.g., in the case of KFe_2As_2 [41] with $I4/mmm$ symmetry. There, the modes involving the K atom located between the Fe_2Se_2 layers are observed only at lower frequencies [Fig. 3(b)]. Such a situation leads to the emergence of nearly flat phonon bands with a weak

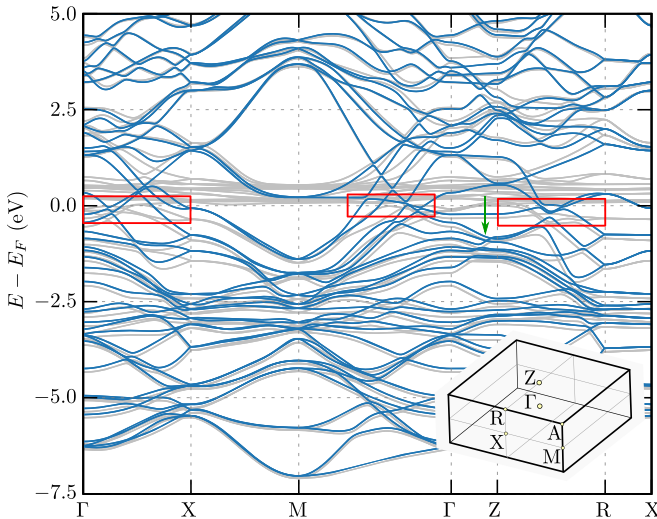


FIG. 4. Electronic band structures of CeRh_2As_2 in the presence of the SOC. Solid blue and gray lines correspond to different treatments of the Ce $4f$ electrons (as core and as valence electrons, respectively).

contribution to lattice thermal conductivity, due to a small group velocity and short phonon lifetime. Moreover, this physical behavior can be examined experimentally by the phonon lifetime measurements [42]. One finds that modes mixing vibrations of Rh and As atoms are of particular interest and are visible in the whole range of the phonon spectrum.

The effect of orbital order on the phonon spectra is noticeable by comparing the results for the $P4/nmm$ and $P4mm$ space groups (without and with orbital order, respectively). By reducing symmetry, we find a small shift of energies and a splitting of phonon branches resulting from a slightly different charge distribution on two sites of the Ce atoms (Fig. S1 in the SM [27]). This effect could be verified in the future by inelastic scattering measurements [43–45].

Electronic band structure. The calculated electronic band structure in the presence of SOC is presented in Fig. 4. The absence of magnetic order in CeRh_2As_2 leads to the spin degeneracy of electronic bands in the $P4/nmm$ symmetry. For instance, at $k_z = 0$ the degeneracy of the bands is preserved at the X and M points. Additionally, along the Γ - Z direction the bands cross below the Fermi level (marked by the green arrow in Fig. 4). Similar behavior is observed in the nonmagnetic Dirac semimetals (with the same symmetry), as in CeSbTe [14]. However, note that the Dirac point and nontrivial topology can be expected even in canonical heavy fermion systems such as CeCoIn_5 [46] with the $P4/mmm$ symmetry.

CeRh_2As_2 can be compared with SrPt_2As_2 [47,48] and LaPt_2Si_2 [48], both crystallizing in the same $P4/nmm$ symmetry. The SOC has a weaker impact on the band structure of CeRh_2As_2 than for SrPt_2As_2 [47,48] and is comparable with the impact on the band structure of LaPt_2Si_2 [48] (cf. Fig. S4 in the SM [27]). These changes can be a consequence of the modifications of chemical composition, due to the mass dependence of the SOC [49,50]. Indeed, the biggest splitting of the bands induced by the SOC is well visible in the

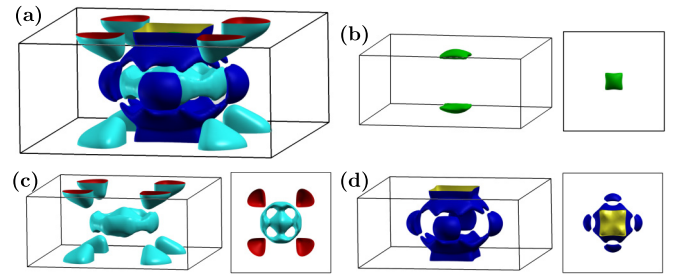


FIG. 5. (a) The Fermi surface of CeRh_2As_2 and (b)–(d) its separate pockets (side and top views). Results were obtained in the presence of SOC and for Ce $4f$ electrons treated as valence electrons.

unoccupied Ce $4f$ energy levels (around 0.25–0.5 eV above the Fermi level).

The band structure shows the shift of the Fermi level in CeRh_2As_2 to lower energies with respect to SrPt_2As_2 [47,48] and LaPt_2Si_2 [48]. In both latter compounds, the band structures around the Fermi level are associated with the atoms located in the layers, i.e., Pt and As in SrPt_2As_2 [47,48], as well as Pt and Si in LaPt_2Si_2 [48]. In our case, the band structure around the Fermi level originates mostly from the Ce $4f$ and Rh $4d$ electrons, which is well visible on the orbital projection of bands (see Fig. S3 in the SM [27]). The Ce $4f$ electrons are located at a relatively small range of energies, which leads to the well visible peak of the density of states (see Fig. S2 in the SM [27]). However, the Rh_2As_2 layers play an important role in the general form of the band structure in CeRh_2As_2 . This is well visible when we compare the band structure of real CeRh_2As_2 with an artificial system without Ce atoms (i.e., containing only two Rh_2As_2 layers) (cf. Fig. S5 in the SM [27]). The main features of the artificial Rh_2As_2 system are conserved and well visible in the band structure of CeRh_2As_2 . The differences arise only from $5d$ electron levels of Ce atoms occupied by one electron.

Fermi surface. The Fermi surface of CeRh_2As_2 [Fig. 5(a)] is composed of three pockets [see Figs. 5(b)–5(d)], which exhibit a three-dimensional (3D) character. Contrary to the other heavy fermion systems, e.g., to CeCoIn_5 [51–57], there is no pocket with quasi-two-dimensional features (i.e., no pockets with a weak z -direction dependence). Theoretical calculations of the electronic structure show that the band structure around the Fermi level can be very sensitive to chemical doping (see the red boxes in Fig. 4). This is associated with a relatively large number of hybridized bands. Similarly, the external magnetic field can lead to a meaningful modification of the electronic structure, as well as of the character of the Fermi pockets.

Role of $4f$ electrons. A comparison of the band structures, when Ce $4f$ electrons are treated as core or valence electrons in the DFT calculations, are shown in Fig. 4 (solid blue and gray lines, respectively). The Ce $4f$ electron energy levels are located around 0.25 and 0.5 eV above the Fermi level, due to the relatively strong SOC [58]. The f - d orbital hybridization leads to a modification of the band structure around the Fermi level. In practice, all energy levels are slightly shifted to lower energies, while the band characters are almost unchanged (cf. gray and blue lines in Fig. 4).

Similarly as in the other heavy fermion systems with $I4/mmm$ symmetry (such as, e.g., URu_2Si_2 [59], CeRh_2Si_2 [60,61], $\text{YbIr}_2\text{Si}_2/\text{YbRh}_2\text{Si}_2$ [62,63], or EuRh_2Si_2 [64–66]), the f - d orbital hybridization can play an important role. Indeed, orbital projected band structures show a strong impact of the Ce $4f$ and Rh $4d$ orbitals onto states around the Fermi level (see Fig. S3 in the SM [27]). This behavior can be important in the context of the correct theoretical description of the studied system and can be indescribable within the simple tight-binding model formulation [1,4,8,67,68]. Additionally, we neglected the role of the strong correlations which can lead to an additional renormalization of the bands, however, this is out of a scope of this Letter and should be a topic of further research. Nevertheless, the exact form of the electronic band structure around the Fermi level should be examined by future investigations within the high-quality angle-resolved photoemission spectroscopy (ARPES) measurements [69–71].

The lattice constants found in the numerical calculations depend on the description of the $4f$ electrons of the Ce atoms (cf. Tables S1–S4 in the SM [27]). Better agreement of the numerical results with experimental data is obtained when the $4f$ electrons are treated as valence electrons. This behavior is well known and associated with the formation of stronger bonding in systems including f electrons, which leads to a decreased volume.

Magnetic instability. The GS found from the *ab initio* calculations is nonmagnetic. However, Ce atoms have nonzero magnetic moments of magnitude below $0.03\mu_B$. This can be a symptom of magnetic instability of the system, which could lead to magnetic ordering at lower temperatures. Regardless of the GS, the numerical calculations with initially enforced different magnetic orders uncover structures with lattice constants better matching the experimental values (cf. Table S3 in the SM [27]). These enforced initial magnetic orders can discriminate between two Ce atomic sites and support the realization of the previously mentioned orbital order. However, this case is out of the scope of this work and should be studied in the future.

Lifshitz transition. We emphasize that several bands are located close to the Fermi level. Here, one should particularly point out the bands with maxima or minima around the Fermi level, i.e., bands inside the red boxes in Fig. 4. An external magnetic field, due to the Zeeman effect and band splitting, can lead to the emergence of a new, fully polarized Fermi pocket, or to the disappearance of the existing one. This phenomenon, called a *magnetic Lifshitz transition* (MLT), was described in the context of a high-magnetic field phase observed in FeSe [72]. During the MLT a modification of the Fermi surface topology is observed, which could be realized here by the external magnetic field [72,73].

To mimic a tendency of CeRh_2As_2 to the realization of MLT, we performed calculations with a nonequal number of spin-up and spin-down electrons, i.e., in a spin-polarized state (cf. Fig. S6 in the SM [27]). For a comparison, we calculated band structures for several values of the spin imbalance. In such a case, we notice two effects: (i) The artificially introduced polarization changes the Fermi level, and (ii) strong modifications of the Fermi pockets even by a small change of

the Fermi level (cf. Fig. S7 in the SM [27]). For example, the smallest Fermi pocket [presented in Fig. 5(b)] can disappear as a result of a shift of the Fermi level by 0.01 eV.

Finally, note that the mentioned shift of the Fermi level by 0.01 eV corresponds to a relatively large external magnetic field. However, one expects that the arising magnetic order may in turn induce a sufficient internal “effective” magnetic field. This resembles the antiferromagnetic-like order in other heavy fermion compounds (in the presence of an external magnetic field). As an example one can mention here the Q phase in CeCoIn_5 [74–76]. We underline that the magnetic field, at which the MLT occurs, has an approximately constant value [72,73,77]. Experimentally, the transition observed in CeRh_2As_2 occurs also at an approximately constant magnetic field [1].

The realization of the MLT can change the topological character of CeRh_2As_2 . Similarly to the above-mentioned case of orbital order, the change in degeneracy or the number of bands crossing directly the Fermi level can change the topological character of the system. Indeed, recently performed theoretical calculations of the \mathbb{Z}_2 invariant based on the tight-binding model support this idea [67]. In such a situation, the realization of a topological surface edge state is expected [67,68], which makes this material interesting also in the context of topological properties or applications.

Conclusions. Summarizing, by using the *ab initio* techniques we investigated the physical properties of the CeRh_2As_2 compound. The specific crystal structure as well as the previous investigations on heavy fermion compounds with the same $P4/nmm$ symmetry suggest a prominent role of the Rh_2As_2 layers in the properties of this compound. Their impact is visible in the phonon spectra, where Ce modes are located only at lower frequencies due to the cagelike structure built by the Rh_2As_2 layers. Additionally, orbital projections of the electronic band structure suggest the strong hybridization between Ce $4f$ and Rh $4d$ electrons. The electronic states located around the Fermi level are mostly composed by orbitals of these types, which may be important for the construction of a realistic tight-binding model of this compound.

Due to the location of Ce atoms between two nonequivalent Rh_2As_2 layers the emergence of the orbital ordering is supported. As a result, two distinguishable Ce sublattices with different effective “orbitals” are found. Similarly as in URu_2As_2 , such orbitals exhibit out-of-plane anisotropy. This orbital order should occur independently of the external magnetic field. Moreover, in practice, this orbital order leads to a lowering of the system symmetry. As a consequence, the measurable modifications of the phonon band degeneracy occur.

From the observed small band splitting we conclude that the spin-orbit coupling is relatively weak. However, the electronic band structure of CeRh_2As_2 reveals specific topological properties of this system. First, we can observe band crossing (the Dirac points), approximately 1 eV below the Fermi level. Second, the bands near the Fermi level support the hypothesis of the magnetic Lifshitz transition. At finite magnetic field, the new fully polarized Fermi pocket could emerge, and the spin-triplet pairing (topological superconducting phase) would arise.

Acknowledgments. We warmly thank Dominik Legut and Dariusz Kaczorowski for insightful discussions. Some figures in this work were rendered using VESTA [78] and XCRYSDEN [79] software. This work was supported by National Science Centre (NCN, Poland) under Projects No. 2016/21/D/ST3/03385 (A.P.), No. 2017/24/C/ST3/00276

(K.J.K.), No. 2016/23/B/ST3/00839 (A.M.O.), and No. 2017/25/B/ST3/02586 (P.P.). In addition, A.P. and K.J.K. are grateful for the funding from the scholarships of the Minister of Science and Higher Education (Poland) for outstanding young scientists (No. 818/STYP/14/2019 and No. 821/STYP/14/2019, respectively).

-
- [1] S. Khim, J. F. Landaeta, J. Banda, N. Bannor, M. Brando, P. M. R. Brydon, D. Hafner, R. Küchler, R. Cardoso-Gil, U. Stockert, A. P. Mackenzie, D. F. Agterberg, C. Geibel, and E. Hassinger, Field-induced transition from even to odd parity superconductivity in CeRh_2As_2 , [arXiv:2101.09522](https://arxiv.org/abs/2101.09522).
- [2] K. Kudo, Y. Nishikubo, and M. Nohara, Coexistence of superconductivity and charge density wave in SrPt_2As_2 , *J. Phys. Soc. Jpn.* **79**, 123710 (2010).
- [3] Y. Nagano, N. Araoka, A. Mitsuda, H. Yayama, H. Wada, M. Ichihara, M. Isobe, and Y. Ueda, Charge density wave and superconductivity of RPt_2Si_2 ($R = \text{Y, La, Nd, and Lu}$), *J. Phys. Soc. Jpn.* **82**, 064715 (2013).
- [4] E. G. Schertenleib, M. H. Fischer, and M. Sigrist, Unusual H - T phase diagram of CeRh_2As_2 : The role of staggered noncentrosymmetry, *Phys. Rev. Research* **3**, 023179 (2021).
- [5] T. Yoshida, M. Sigrist, and Y. Yanase, Parity-mixed superconductivity in locally non-centrosymmetric system, *J. Phys. Soc. Jpn.* **83**, 013703 (2014).
- [6] D. Möckli and M. Khodas, Robust parity-mixed superconductivity in disordered monolayer transition metal dichalcogenides, *Phys. Rev. B* **98**, 144518 (2018).
- [7] D. Möckli and M. Khodas, Magnetic-field induced $s + if$ pairing in Ising superconductors, *Phys. Rev. B* **99**, 180505(R) (2019).
- [8] D. Möckli and A. Ramires, Two scenarios for superconductivity in CeRh_2As_2 , *Phys. Rev. Research* **3**, 023204 (2021).
- [9] S. M. Young and C. L. Kane, Dirac Semimetals in Two Dimensions, *Phys. Rev. Lett.* **115**, 126803 (2015).
- [10] L. M. Schoop, M. N. Ali, C. Straßer, A. Topp, A. Varykhalov, D. Marchenko, V. Duppel, S. S. P. Parkin, B. V. Lotsch, and C. R. Ast, Dirac cone protected by non-symmorphic symmetry and three-dimensional Dirac line node in ZrSiS , *Nat. Commun.* **7**, 11696 (2016).
- [11] D. Takane, Zhiwei Wang, S. Souma, K. Nakayama, C. X. Trang, T. Sato, T. Takahashi, and Y. Ando, Dirac-node arc in the topological line-node semimetal HfSiS , *Phys. Rev. B* **94**, 121108(R) (2016).
- [12] M. M. Hosen, K. Dimitri, I. Belopolski, P. Maldonado, R. Sankar, N. Dhakal, G. Dhakal, T. Cole, P. M. Oppeneer, D. Kaczorowski, F. Chou, M. Z. Hasan, T. Durakiewicz, and M. Neupane, Tunability of the topological nodal-line semimetal phase in ZrSiX -type materials ($X = \text{S, Se, Te}$), *Phys. Rev. B* **95**, 161101(R) (2017).
- [13] C. Chen, X. Xu, J. Jiang, S.-C. Wu, Y. P. Qi, L. X. Yang, M. X. Wang, Y. Sun, N. B. M. Schröter, H. F. Yang, L. M. Schoop, Y. Y. Lv, J. Zhou, Y. B. Chen, S. H. Yao, M. H. Lu, Y. F. Chen, C. Felser, B. H. Yan, Z. K. Liu *et al.*, Dirac line nodes and effect of spin-orbit coupling in the nonsymmorphic critical semimetals $M\text{SiS}$ ($M = \text{Hf, Zr}$), *Phys. Rev. B* **95**, 125126 (2017).
- [14] L. M. Schoop, A. Topp, J. Lippmann, F. Orlandi, L. MÜchler, M. G. Vergniory, Y. Sun, A. W. Rost, V. Duppel, M. Krivenkov, S. Sheoran, P. Manuel, A. Varykhalov, B. Yan, R. K. Kremer, C. R. Ast, and B. V. Lotsch, Tunable Weyl and Dirac states in the nonsymmorphic compound CeSbTe , *Sci. Adv.* **4**, eaar2317 (2018).
- [15] S. Pezzini, M. R. van Delft, L. M. Schoop, B. V. Lotsch, A. Carrington, M. I. Katsnelson, N. E. Hussey, and S. Wiedmann, Unconventional mass enhancement around the Dirac nodal loop in ZrSiS , *Nat. Phys.* **14**, 178 (2018).
- [16] Y.-Y. Wang, S. Xu, L.-L. Sun, and T.-L. Xia, Quantum oscillations and coherent interlayer transport in a new topological Dirac semimetal candidate YbMnSb_2 , *Phys. Rev. Mater.* **2**, 021201(R) (2018).
- [17] S. Klemenz, S. Lei, and L. M. Schoop, Topological semimetals in square-net materials, *Annu. Rev. Mater. Res.* **49**, 185 (2019).
- [18] G. Kresse and J. Hafner, *Ab initio* molecular-dynamics simulation of the liquid-metal–amorphous-semiconductor transition in germanium, *Phys. Rev. B* **49**, 14251 (1994).
- [19] G. Kresse and J. Furthmüller, Efficient iterative schemes for *ab initio* total-energy calculations using a plane-wave basis set, *Phys. Rev. B* **54**, 11169 (1996).
- [20] G. Kresse and D. Joubert, From ultrasoft pseudopotentials to the projector augmented-wave method, *Phys. Rev. B* **59**, 1758 (1999).
- [21] T. Tadano, Y. Gohda, and S. Tsuneyuki, Anharmonic force constants extracted from first-principles molecular dynamics: applications to heat transfer simulations, *J. Phys.: Condens. Matter* **26**, 225402 (2014).
- [22] P. T. Jochym and J. Łażewski, High Efficiency Configuration Space Sampling – probing the distribution of available states, *SciPost Phys.* **10**, 129 (2021).
- [23] P. E. Blöchl, Projector augmented-wave method, *Phys. Rev. B* **50**, 17953 (1994).
- [24] J. P. Perdew, K. Burke, and M. Ernzerhof, Generalized Gradient Approximation Made Simple, *Phys. Rev. Lett.* **77**, 3865 (1996).
- [25] J. P. Perdew, A. Ruzsinszky, G. I. Csonka, O. A. Vydrov, G. E. Scuseria, L. A. Constantin, X. Zhou, and K. Burke, Restoring the Density-Gradient Expansion for Exchange in Solids and Surfaces, *Phys. Rev. Lett.* **100**, 136406 (2008).
- [26] H. J. Monkhorst and J. D. Pack, Special points for Brillouin-zone integrations, *Phys. Rev. B* **13**, 5188 (1976).
- [27] See Supplemental Material at <http://link.aps.org/supplemental/10.1103/PhysRevB.104.L041109> for the description of numerical methods details, additional numerical results discussing: lattice constants, band structure, phonons spectra and Lifshitz transition.
- [28] Q. G. Mu, B. J. Pan, B. B. Ruan, T. Liu, K. Zhao, L. Shan, G. F. Chen, and Z. A. Ren, Superconductivity in LaPd_2Bi_2 with

- CaBe₂Ge₂-type structure, *Sci. China Phys. Mech. Astron.* **61**, 127409 (2018).
- [29] E. M. Nica, R. Yu, and Q. Si, Glide reflection symmetry, Brillouin zone folding, and superconducting pairing for the $P4/nmm$ space group, *Phys. Rev. B* **92**, 174520 (2015).
- [30] R. Nourafkan and A.-M. S. Tremblay, Effect of nonsymmorphic space groups on correlation functions in iron-based superconductors, *Phys. Rev. B* **96**, 125140 (2017).
- [31] V. Cvetkovic and O. Vafek, Space group symmetry, spin-orbit coupling, and the low-energy effective Hamiltonian for iron-based superconductors, *Phys. Rev. B* **88**, 134510 (2013).
- [32] S. Sumita and Y. Yanase, Unconventional superconducting gap structure protected by space group symmetry, *Phys. Rev. B* **97**, 134512 (2018).
- [33] A. D. Becke and K. E. Edgecombe, A simple measure of electron localization in atomic and molecular systems, *J. Chem. Phys.* **92**, 5397 (1990).
- [34] A. Savin, O. Jepsen, J. Flad, O. K. Andersen, H. Preuss, and H. G. von Schnering, Electron localization in solid-state structures of the elements: The diamond structure, *Angew. Chem., Int. Ed. Engl.* **31**, 187 (1992).
- [35] B. Silvi and A. Savin, Classification of chemical bonds based on topological analysis of electron localization functions, *Nature (London)* **371**, 683 (1994).
- [36] P. Chandra, P. Coleman, J. A. Mydosh, and V. Tripathi, Hidden orbital order in the heavy fermion metal URu₂Si₂, *Nature (London)* **417**, 831 (2002).
- [37] M. Sundermann, M. W. Haverkort, S. Agrestini, A. Al-Zein, M. Moretti Sala, Y. Huang, M. Golden, A. de Visser, P. Thalmeier, L. H. Tjeng, and A. Severing, Direct bulk-sensitive probe of $5f$ symmetry in URu₂Si₂, *Proc. Natl. Acad. Sci. USA* **113**, 13989 (2016).
- [38] H.-H. Kung, R. E. Baumbach, E. D. Bauer, V. K. Thorsmølle, W.-L. Zhang, K. Haule, J. A. Mydosh, and G. Blumberg, Chirality density wave of the “hidden order” phase in URu₂Si₂, *Science* **347**, 1339 (2015).
- [39] M. Z. Hasan and C. L. Kane, Colloquium: Topological insulators, *Rev. Mod. Phys.* **82**, 3045 (2010).
- [40] T. Takabatake, K. Suekuni, T. Nakayama, and E. Kaneshita, Phonon-glass electron-crystal thermoelectric clathrates: Experiments and theory, *Rev. Mod. Phys.* **86**, 669 (2014).
- [41] A. Ptok, M. Sternik, K. J. Kapcia, and P. Piekarczyk, Structural, electronic, and dynamical properties of the tetragonal and collapsed tetragonal phases of KFe₂As₂, *Phys. Rev. B* **99**, 134103 (2019).
- [42] P.-F. Lory, S. Pailhès, V. M. Giordano, H. Euchner, H. D. Nguyen, R. Ramlau, H. Borrmann, M. Schmidt, M. Baitinger, M. Ikeda, P. Tomeš, M. Mihalkovič, C. Allio, M. R. Johnson, H. Schober, Y. Sidis, F. Bourdarot, L. P. Regnault, J. Ollivier, S. Paschen *et al.*, Direct measurement of individual phonon lifetimes in the clathrate compound Ba_{7.81}Ge_{40.67}Au_{5.33}, *Nat. Commun.* **8**, 491 (2017).
- [43] O. Delaire, J. Ma, K. Marty, A. F. May, M. A. McGuire, M.-H. Du, D. J. Singh, A. Podlesnyak, G. Ehlers, M. D. Lumsden, and B. C. Sales, Giant anharmonic phonon scattering in PbTe, *Nat. Mater.* **10**, 614 (2011).
- [44] J. Ma, O. Delaire, A. F. May, C. E. Carlton, M. A. McGuire, L. H. VanBebber, D. L. Abernathy, G. Ehlers, T. Hong, A. Huq, W. Tian, V. M. Keppens, Y. Shao-Horn, and B. C. Sales, Glass-like phonon scattering from a spontaneous nanostructure in AgSbTe₂, *Nat. Nanotech.* **8**, 445 (2013).
- [45] C. W. Li, J. Hong, A. F. May, D. Bansal, S. Chi, T. Hong, G. Ehlers, and O. Delaire, Orbitally driven giant phonon anharmonicity in SnSe, *Nat. Phys.* **11**, 1063 (2015).
- [46] K. R. Shirer, Y. Sun, M. D. Bachmann, C. Putzke, T. Helm, L. E. Winter, F. F. Balakirev, R. D. McDonald, J. G. Analytis, N. L. Nair, E. D. Bauer, F. Ronning, C. Felser, T. Meng, B. Yan, and P. J. W. Moll, Dirac fermions in the heavy-fermion superconductors Ce(Co,Rh,Ir)In₅, [arXiv:1808.00403](https://arxiv.org/abs/1808.00403).
- [47] I. A. Nekrasov and M. V. Sadovskii, Electronic structure of novel multiple-band superconductor SrPt₂As₂, *JETP Lett.* **92**, 751 (2010).
- [48] S. Kim, K. Kim, and B. I. Min, The mechanism of charge density wave in Pt-based layered superconductors: SrPt₂As₂ and LaPt₂Si₂, *Sci. Rep.* **5**, 15052 (2015).
- [49] F. Herman, C. D. Kuglin, K. F. Cuff, and R. L. Kortum, Relativistic Corrections to the Band Structure of Tetrahedrally Bonded Semiconductors, *Phys. Rev. Lett.* **11**, 541 (1963).
- [50] K. V. Shanavas, Z. S. Popović, and S. Satpathy, Theoretical model for Rashba spin-orbit interaction in d electrons, *Phys. Rev. B* **90**, 165108 (2014).
- [51] R. Settai, H. Shishido, S. Ikeda, Y. Murakawa, M. Nakashima, D. Aoki, Y. Haga, H. Harima, and Y. Onuki, Quasi-two-dimensional Fermi surfaces and the de Haas–van Alphen oscillation in both the normal and superconducting mixed states of CeCoIn₅, *J. Phys.: Condens. Matter* **13**, L627 (2001).
- [52] H. Shishido, R. Settai, D. Aoki, Shugo Ikeda, H. Nakawaki, N. Nakamura, T. Iizuka, Y. Inada, K. Sugiyama, T. Takeuchi, K. Kindo, T. C. Kobayashi, Y. Haga, H. Harima, Y. Aoki, T. Namiki, H. Sato, and Y. Onuki, Fermi surface, magnetic and superconducting properties of LaRhIn₅ and CeTIn₅ (T : Co, Rh and Ir), *J. Phys. Soc. Jpn.* **71**, 162 (2002).
- [53] T. Maehira, T. Hotta, K. Ueda, and A. Hasegawa, Relativistic band-structure calculations for CeTIn₅ (T = Ir and Co) and analysis of the energy bands by using tight-binding method, *J. Phys. Soc. Jpn.* **72**, 854 (2003).
- [54] P. M. Oppeneer, S. Elgazzar, A.B. Shick, I. Opahle, J. Ruzs, and R. Hayn, Fermi surface changes due to localized–delocalized f -state transitions in Ce-115 and Pu-115 compounds, *J. Magn. Magn. Mater.* **310**, 1684 (2007).
- [55] F. Ronning, J.-X. Zhu, T. Das, M. J. Graf, R. C. Albers, H. B. Rhee, and W. E. Pickett, Superconducting gap structure of the 115s revisited, *J. Phys.: Condens. Matter* **24**, 294206 (2012).
- [56] A. Polyakov, O. Ignatchik, B. Bergk, K. Götze, A. D. Bianchi, S. Blackburn, B. Prévost, G. Seyfarth, M. Côté, D. Hurt, C. Capan, Z. Fisk, R. G. Goodrich, I. Sheikin, M. Richter, and J. Wosnitza, Fermi-surface evolution in Yb-substituted CeCoIn₅, *Phys. Rev. B* **85**, 245119 (2012).
- [57] A. Ptok, K. J. Kapcia, P. Piekarczyk, and A. M. Oleś, The *ab initio* study of unconventional superconductivity in CeCoIn₅ and FeSe, *New J. Phys.* **19**, 063039 (2017).
- [58] We also compared the electronic band structure from VASP with results obtained within QUANTUM ESPRESSO software [80,81] and pseudopotentials developed in a frame of PSLIBRARY [82]. One needs to notice that the Ce atoms in both cases have different electronic configurations, i.e., [Xe] 6s²4f^{0.5}5d^{1.5} in the case of PSLIBRARY and [Xe] 6s²4f¹5d¹ for VASP pseudopotentials. In consequence, the Ce 4f electron levels can be overestimated (cf. Fig. 4 and Fig. S8 in the SM [27]).

- [59] H. Ikeda, M.-T. Suzuki, R. Arita, and T. Takimoto, Multipole fluctuations of itinerant f electrons and trikontadipole order in URu₂Si₂, *C. R. Phys.* **15**, 587 (2014).
- [60] S. Patil, A. Generalov, M. Güttler, P. Kushwaha, A. Chikina, K. Kummer, T. C. Rödel, A. F. Santander-Syro, N. Caroca-Canales, C. Geibel, S. Danzenbächer, Y. Kucherenko, C. Laubschat, J. W. Allen, and D. V. Vyalikh, ARPES view on surface and bulk hybridization phenomena in the antiferromagnetic Kondo lattice CeRh₂Si₂, *Nat. Commun.* **7**, 11029 (2016).
- [61] G. Poelchen, S. Schulz, M. Mende, M. Güttler, A. Generalov, A. V. Fedorov, N. Caroca-Canales, Ch. Geibel, K. Kliemt, C. Krellner, S. Danzenbächer, D. Y. Usachov, P. Dudin, V. N. Antonov, J. W. Allen, C. Laubschat, K. Kummer, Y. Kucherenko, and D. V. Vyalikh, Unexpected differences between surface and bulk spectroscopic and implied Kondo properties of heavy fermion CeRh₂Si₂, *npj Quantum Mater.* **5**, 70 (2020).
- [62] S. Danzenbächer, Y. Kucherenko, D. V. Vyalikh, M. Holder, C. Laubschat, A. N. Yaresko, C. Krellner, Z. Hussain, C. Geibel, X. J. Zhou, W. L. Yang, N. Mannella, Z. Hussain, Z.-X. Shen, M. Shi, L. Patthey, and S. L. Molodtsov, Momentum dependence of $4f$ hybridization in heavy-fermion compounds: Angle-resolved photoemission study of YbIr₂Si₂ and YbRh₂Si₂, *Phys. Rev. B* **75**, 045109 (2007).
- [63] D. V. Vyalikh, S. Danzenbächer, Y. Kucherenko, K. Kummer, C. Krellner, C. Geibel, M. G. Holder, T. K. Kim, C. Laubschat, M. Shi, L. Patthey, R. Follath, and S. L. Molodtsov, k Dependence of the Crystal-Field Splittings of $4f$ States in Rare-Earth Systems, *Phys. Rev. Lett.* **105**, 237601 (2010).
- [64] M. Höppner, S. Seiro, A. Chikina, A. Fedorov, M. Güttler, S. Danzenbächer, A. Generalov, K. Kummer, S. Patil, S. L. Molodtsov, Y. Kucherenko, C. Geibel, V. N. Strocov, M. Shi, M. Radovic, T. Schmitt, C. Laubschat, and D. V. Vyalikh, Interplay of Dirac fermions and heavy quasi-particles in solids, *Nat. Commun.* **4**, 1646 (2013).
- [65] A. Chikina, M. Höppner, S. Seiro, K. Kummer, S. Danzenbächer, S. Patil, A. Generalov, M. Güttler, Y. Kucherenko, E. V. Chulkov, Y. M. Koroteev, K. Koepernik, C. Geibel, M. Shi, M. Radovic, C. Laubschat, and D. V. Vyalikh, Strong ferromagnetism at the surface of an antiferromagnet caused by buried magnetic moments, *Nat. Commun.* **5**, 3171 (2014).
- [66] M. Güttler, A. Generalov, S. I. Fujimori, K. Kummer, A. Chikina, S. Seiro, S. Danzenbächer, Y. M. Koroteev, E. V. Chulkov, M. Radovic, M. Shi, N. C. Plumb, C. Laubschat, J. W. Allen, C. Krellner, C. Geibel, and D. V. Vyalikh, Divalent EuRh₂Si₂ as a reference for the Luttinger theorem and antiferromagnetism in trivalent heavy-fermion YbRh₂Si₂, *Nat. Commun.* **10**, 796 (2019).
- [67] K. Nogaki, A. Daido, J. Ishizuka, and Y. Yanase, Topological crystalline superconductivity in locally noncentrosymmetric CeRh₂As₂, [arXiv:2103.08088](https://arxiv.org/abs/2103.08088).
- [68] D. C. Cavanagh, T. Shishidou, M. Weinert, P. M. R. Brydon, and D. F. Agterberg, Non-symmorphic symmetry and field-driven odd-parity pairing in CeRh₂As₂, [arXiv:2106.02698](https://arxiv.org/abs/2106.02698).
- [69] A. Damascelli, Z. Hussain, and Z.-X. Shen, Angle-resolved photoemission studies of the cuprate superconductors, *Rev. Mod. Phys.* **75**, 473 (2003).
- [70] J. H. Dil, Spin and angle resolved photoemission on non-magnetic low-dimensional systems, *J. Phys.: Condens. Matter* **21**, 403001 (2009).
- [71] B. Lv, T. Qian, and H. Ding, Angle-resolved photoemission spectroscopy and its application to topological materials, *Nat. Rev. Phys.* **1**, 609 (2019).
- [72] A. Ptok, K. J. Kapcia, A. Cichy, A. M. Oleś, and P. Piekarczyk, Magnetic Lifshitz transition and its consequences in multi-band iron-based superconductors, *Sci. Rep.* **7**, 41979 (2017).
- [73] R. Daou, C. Bergemann, and S. R. Julian, Continuous evolution of the Fermi surface of CeRu₂Si₂ across the metamagnetic transition, *Phys. Rev. Lett.* **96**, 026401 (2006).
- [74] M. Kenzelmann, T. Strässle, C. Niedermayer, M. Sigrist, B. Padmanabhan, M. Zolliker, A. D. Bianchi, R. Movshovich, E. D. Bauer, J. L. Sarrao, and J. D. Thompson, Coupled superconducting and magnetic order in CeCoIn₅, *Science* **321**, 1652 (2008).
- [75] M. Kenzelmann, S. Gerber, N. Egetenmeyer, J. L. Gavilano, T. Strässle, A. D. Bianchi, E. Ressouche, R. Movshovich, E. D. Bauer, J. L. Sarrao, and J. D. Thompson, Evidence for a Magnetically Driven Superconducting Q Phase of CeCoIn₅, *Phys. Rev. Lett.* **104**, 127001 (2010).
- [76] G. Koutroulakis, M. D. Stewart, V. F. Mitrović, M. Horvatić, C. Berthier, G. Lapertot, and J. Flouquet, Field Evolution of Coexisting Superconducting and Magnetic Orders in CeCoIn₅, *Phys. Rev. Lett.* **104**, 087001 (2010).
- [77] P. Schlottmann, Lifshitz transition with interactions in high magnetic fields, *Phys. Rev. B* **83**, 115133 (2011).
- [78] K. Momma and F. Izumi, VESTA3 for three-dimensional visualization of crystal, volumetric and morphology data, *J. Appl. Crystallogr.* **44**, 1272 (2011).
- [79] A. Kokalj, XCrySDen—a new program for displaying crystalline structures and electron densities, *J. Mol. Graph. Model.* **17**, 176 (1999).
- [80] P. Giannozzi, S. Baroni, N. Bonini, M. Calandra, R. Car, C. Cavazzoni, D. Ceresoli, G. L. Chiarotti, M. Cococcioni, I. Dabo, A. Dal Corso, S. de Gironcoli, S. Fabris, G. Fratesi, R. Gebauer, U. Gerstmann, C. Gougoussis, A. Kokalj, M. Lazzeri, L. Martin-Samos *et al.*, QUANTUM ESPRESSO: A modular and open-source software project for quantum simulations of materials, *J. Phys.: Condens. Matter* **21**, 395502 (2009).
- [81] P. Giannozzi, O. Andreussi, T. Brumme, O. Bunau, M. Buongiorno Nardelli, M. Calandra, R. Car, C. Cavazzoni, D. Ceresoli, M. Cococcioni, N. Colonna, I. Carnimeo, A. Dal Corso, S. de Gironcoli, P. Delugas, R. A. DiStasio, A. Ferretti, A. Floris, G. Fratesi, G. Fugallo *et al.*, Advanced capabilities for materials modelling with Quantum ESPRESSO, *J. Phys.: Condens. Matter* **29**, 465901 (2017).
- [82] A. Dal Corso, Pseudopotentials periodic table: From H to Pu, *Comput. Mater. Sci.* **95**, 337 (2014).